

Tensile GaAs(111) quantum dashes with tunable luminescence below the bulk bandgap

Christopher D. Yerino,^{1,a)} Paul J. Simmonds,² Baolai Liang,² Vitaliy G. Dorogan,³ Morgan E. Ware,³ Yuriy I. Mazur,³ Daehwan Jung,¹ Diana L. Huffaker,^{2,4} Gregory J. Salamo,³ and Minjoo Larry Lee¹

¹Department of Electrical Engineering, Yale University, New Haven, Connecticut 06520, USA

²California NanoSystems Institute, University of California, Los Angeles, California 90095, USA

³Institute for Nanoscience and Engineering, University of Arkansas, Fayetteville, Arkansas 72701, USA

⁴Department of Electrical Engineering, University of California, Los Angeles, California 90095, USA

(Received 12 June 2014; accepted 11 August 2014; published online 21 August 2014)

Strain-based band engineering in quantum dots and dashes has been predominantly limited to compressively strained systems. However, tensile strain strongly reduces the bandgaps of nanostructures, enabling nanostructures to emit light at lower energies than they could under compressive strain. We demonstrate the self-assembled growth of dislocation-free GaAs quantum dashes on an InP(111)B substrate, using a 3.8% tensile lattice-mismatch. Due to the high tensile strain, the GaAs quantum dashes luminesce at 110–240 meV below the bandgap of bulk GaAs. The emission energy is readily tuned by adjusting the size of the quantum dashes via deposition thickness. Tensile self-assembly creates new opportunities for engineering the band alignment, band structure, and optical properties of epitaxial nanostructures. © 2014 AIP Publishing LLC.

[<http://dx.doi.org/10.1063/1.4893747>]

Strain engineering is a valuable tool for improving the performance of optoelectronic devices and tuning their optical characteristics. These benefits arise from the dramatic band structure transformation that occurs as increasing strain is applied to a semiconductor. In laser diodes, for example, the selection of tensile or compressive strain can improve lasing thresholds^{1,2} and tune the lasing polarization³ by modifying the valence sub-bands. Application of tensile strain has even enabled germanium lasers by enhancing direct optical transitions in the normally indirect bandgap material.⁴ In the case of quantum dots (QDs) and quantum dashes (Q-dashes), despite their important contributions to optoelectronics and quantum information,^{5,6} only two strain states can be reliably prepared: zero strain and compressive strain. To date, the only tensile system that produces optically-active, dislocation-free, (001) QDs is GaAs/GaSb with type-II band alignment.⁷ The inability to grow dislocation-free tensile nanostructures from other materials^{8,9} limits the use of band structure engineering in QD and Q-dash devices.

In particular, nanostructures could experience large bandgap reductions under tensile strain that cannot be achieved by other techniques. The compressive strain used in conventional Stranski-Krastanov growth on (001) surfaces increases the bulk bandgaps of III-V materials by 0.05–0.2 eV, given a typical 4% biaxial strain.¹⁰ In contrast, tensile strain *lowers* bandgaps below their bulk values, with reductions of 0.4–0.6 eV for III-Vs under 4% tension (or 0.5–0.8 eV on (111) surfaces).¹⁰ Signorello *et al.* performed experiments to mechanically stretch nanowires, and found that 3.5% uniaxial tension can red-shift the photoluminescence (PL) emission energy of a GaAs/AlGaAs nanowire by nearly 300 meV.¹¹ We recently demonstrated that tensile

GaAs (110) QDs exhibit a similar bandgap reduction without external manipulation, obtaining PL emission 240 meV below the bulk bandgap.¹² These levels of strain, while common to nanostructures, are difficult to incorporate elastically into quantum wells due to the low critical thickness for dislocation nucleation that results. Tensile strain thus provides a means to produce nanostructures with much lower bandgaps than previously available, providing access to lower emission energies for photonic devices.

In this work, we demonstrate the self-assembly of optically active, tensile strained GaAs Q-dashes on an InP(111)B substrate. Our results show that the (111) surface is favorable for dislocation-free, tensile self-assembly, as predicted by our recent growth model.⁹ Type-I quantum confinement of carriers is achieved by growing the GaAs Q-dashes within an In_{0.52}Al_{0.48}As matrix (InAlAs), while the 3.8% tensile strain substantially lowers the GaAs bandgap (Fig. 1). In the absence of dislocations, the (111)B Q-dashes exhibit strong PL at room temperature. Due to the high tensile strain, PL energies 110–240 meV *below* the bulk bandgap of GaAs are observed. The strong reduction in PL emission energy, despite the quantum confinement effect, demonstrates the large bandgap tunability that can be achieved using tensile strained nanostructures.

The band alignments for the GaAs/InAlAs(111)B Q-dashes are shown in Fig. 1. The values shown were calculated from model-solid theory¹³ using band parameters and elastic constants from Vurgaftman *et al.*¹⁴ For GaAs fully strained to the InAlAs(111)B, the 3.8% biaxial tension lowers the GaAs bandgap by 0.7 eV, providing type-I confinement for both electrons and holes. The actual transition energies will lie higher than the calculated bandgap in Fig. 1 as a result of both quantum confinement in the Q-dashes and partial elastic relaxation from the 3D self-assembly

^{a)}Electronic mail: christopher.yerino@yale.edu

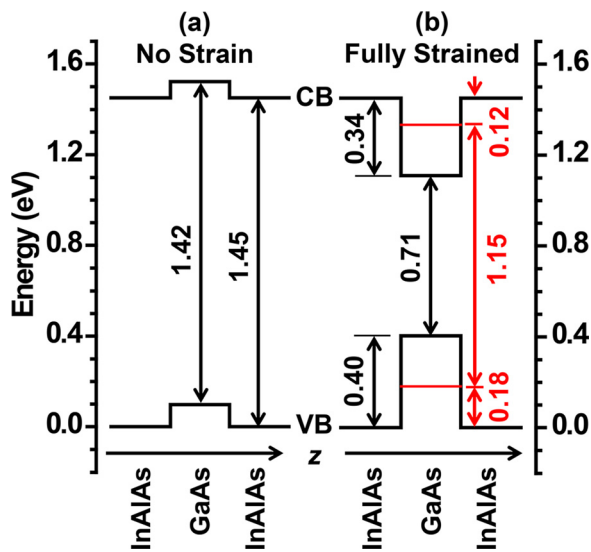


FIG. 1. Band alignment calculations for GaAs layers within $\text{In}_{0.52}\text{Al}_{0.48}\text{As}(111)\text{B}$ at 300 K, comparing the alignment (a) without strain present and (b) with GaAs fully and biaxially strained to the InAlAs. In (b), the GaAs bandgap is lowered by 0.7 eV due to tensile strain, producing type-I confinement for electrons and holes. Red lines indicate ground states for Q-dashes formed from 3 ML thick GaAs (with dimensions from TEM images in Fig. 3). All energies are given in eV.

process.¹⁵ Nonetheless, this model predicts that the recombination energies in the GaAs nanostructures remain smaller than the bulk bandgap of GaAs.

Samples are grown in a VEECO Modular GEN II solid-source molecular beam epitaxy system (MBE), using P_2 and As_4 as the group-V sources. We use semi-insulating $\text{InP}(111)\text{B}$ substrates offcut 2° toward $(2\bar{1}\bar{1})$. This particular offcut prevents faceting during growth of InAlAs, InGaAs, and other III-Vs on (111)B.¹⁶ The native oxide is desorbed at 500°C under P_2 , followed by the growth of 5 nm InAlAs at 480°C and 200–500 nm InAlAs at 540°C (all temperatures are measured by optical pyrometer). The high InAlAs growth temperature prevents formation of step bunches that would otherwise roughen the surface. A narrow growth window with a V/III beam equivalent pressure ratio of ~ 10 produces an optimally smooth surface (Fig. 2(a)) with root mean square (rms) roughness of 0.44 nm over a $15 \times 15 \mu\text{m}^2$ area. Higher or lower V/III ratios increase the roughness substantially. Due to the high desorption rate of indium at 540°C ,¹⁷ the InAlAs composition is sensitive to small temperature variations. Thus, the $\text{In}_x\text{Al}_{1-x}\text{As}$ composition varies among samples from $x = 0.514$ – 0.525 as measured by x-ray diffraction and PL. Following the InAlAs buffer growth, 0–4 ML of GaAs(111)B is deposited at 515°C at a growth rate of 0.09 ML/s with a V/III ratio of 30. After GaAs deposition, samples are either cooled in As_4 for observation by atomic force microscope (AFM), or the GaAs is capped with 100 nm InAlAs for PL and transmission electron microscopy (TEM). The first 10 nm of the InAlAs cap is grown at 515°C , followed by 90 nm of InAlAs at 540°C . PL measurements are performed by focusing a 532 nm laser onto each sample and measuring the PL signal with an InGaAs detector. The polarization dependence of the PL was measured by passing the PL signal through a rotation-mounted half-waveplate and a fixed polarizing filter prior to the detector. TEM is performed

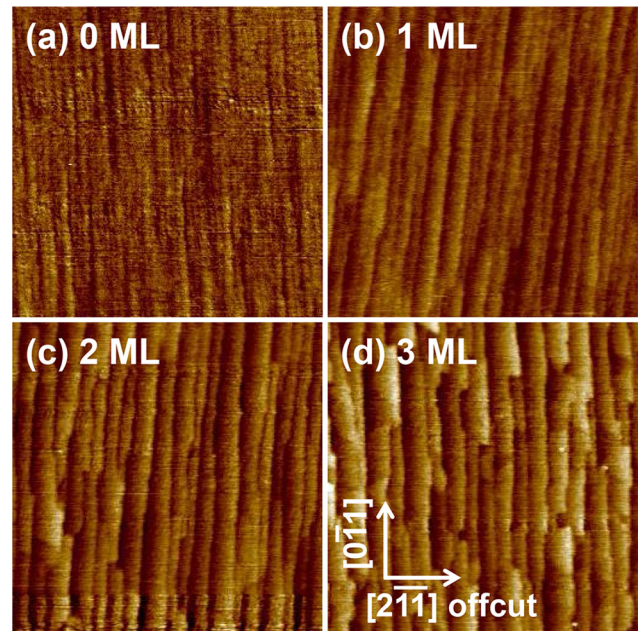


FIG. 2. AFM images of uncapped GaAs layers, $0.5 \times 0.5 \mu\text{m}^2$ in area, grown on $\text{InAlAs}(111)\text{B}$: (a) bare InAlAs buffer, (b) 1 ML GaAs, (c) 2 ML GaAs, and (d) 3 ML GaAs layers. The height scale is 3 nm.

in both cross-section (X-TEM) and plan-view (PV-TEM) using a FEI Osiris operating at 200 keV.

AFM imaging of the uncapped GaAs layers shows that nanostructure morphology is directed by the substrate offcut (Fig. 2). The vicinal growth produces nearly straight terraces perpendicular to the 2° offcut, running parallel to $[0\bar{1}1]$. Prior to GaAs growth, the InAlAs buffer terraces have an average width of 11 nm, consistent with monolayer-high steps and the 2° offcut (Fig. 2(a)). GaAs deposited on the offcut InAlAs produces wider, taller, parallel steps as a result of step-bunching. During the first 1 ML of GaAs deposition, many of the monolayer-high steps merge into bi-layer steps. These steps increase in spacing and height with increased GaAs deposition. By 2 ML, the size distributions of the GaAs terraces are 26 ± 8 nm wide and 0.76 ± 0.31 nm tall, while the 3 ML terraces are 34 ± 14 nm wide and 0.86 ± 0.47 nm tall. The increase in step spacing and height with GaAs deposition indicates that neighboring steps are merging together to form macrosteps as the growth progresses. These straight, parallel surface undulations are similar to earlier work on wire-like GaAs/AlGaAs structures grown on highly offcut wafers.¹⁸ In those studies, macrosteps were formed intentionally on the offcut AlGaAs, followed by the selective growth of GaAs wires at the steps. Our present results exhibit a different growth mechanism, where macrosteps form upon deposition of tensile GaAs onto a smooth, monolayer-stepped offcut surface.

TEM imaging shows the morphology and structural quality of the buried GaAs nanostructures. The buried GaAs layers (Figs. 3(b)–3(d)) each exhibit wire-like strain contrast features that are not present in the InAlAs reference sample (Fig. 3(a)). These features are ~ 50 – 400 nm long for all samples and are ~ 6 – 10 nm wide. We designate these nanostructures as Q-dashes due to their size range and large anisotropy.¹⁹ As more GaAs is deposited, the strain contrast

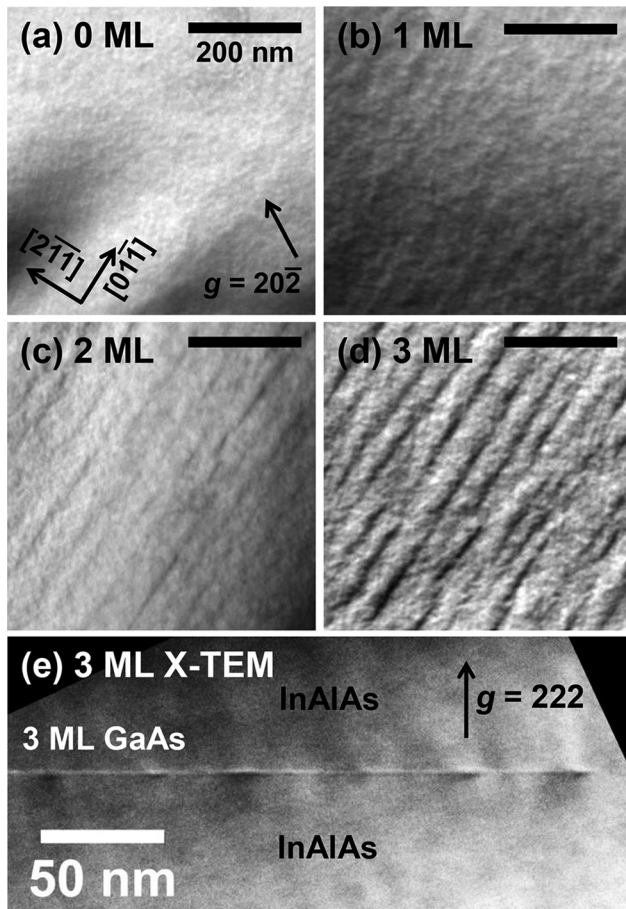


FIG. 3. Bright-field TEM images of GaAs Q-dashes surrounded by InAlAs barriers. PV-TEM images are shown for (a) a bare InAlAs buffer, (b) 1 ML GaAs, (c) 2 ML GaAs, and (d) 3 ML GaAs layers. Images (a)–(d) all use a 200 nm scale bar and $g = 20\bar{2}$ as shown in (a). (e) X-TEM of the 3 ML GaAs layer using the $[0\bar{1}1]$ imaging zone; the long axes of the Q-dashes are perpendicular to the page.

becomes stronger, suggesting that the Q-dashes become thicker in the out-of plane direction. The density of the Q-dashes remains constant at $8 \times 10^9 \text{ cm}^{-2}$ as GaAs thickness increases, maintaining a lateral spacing of $41 \pm 12 \text{ nm}$ between adjacent Q-dashes. This behavior differs from the morphology of the uncapped GaAs (Fig. 2), which has a smaller macrostep spacing that increases with GaAs thickness. This complex change in Q-dash density resembles the restructuring of QDs that commonly occurs during capping, whereby mass transport during cap deposition changes the size, shape, and density of the QDs.²⁰ X-TEM on the 3 ML Q-dash sample was performed along the $[0\bar{1}1]$ zone by preparing a thin section parallel to the offcut direction (Fig. 3(e)). The points of strain contrast have identical spacing to the Q-dashes seen in PV-TEM and confirm that the dashes are aligned along $[0\bar{1}1]$, parallel to the offcut steps. The substrate offcut thus guides the growth of the Q-dashes, likely by the formation of macrosteps that restructure during capping.

The TEM images show that GaAs layers $\leq 3 \text{ ML}$ thick incorporate the 3.8% tensile strain elastically without nucleating dislocations (Fig. 3). This observation is consistent with our model's prediction that (111) surfaces can accommodate large tensile strains.⁹ However, when the GaAs

thickness is increased to 4 ML, the accumulated strain energy exceeds the threshold for dislocations, as observed by TEM (see supplementary material²¹). Similar limits to dislocation-free deposition thickness are present in conventional QD growth.²² The high crystalline quality of the 1–3 ML tensile GaAs(111)B growths contrasts strongly with tensile growth on most (001) surfaces under similar strains, where dislocation-free nanostructures are difficult to obtain.⁸ Dislocation free tensile nanostructures were similarly observed for GaP on GaAs(111)A²³ and Si on Ge(111),²⁴ suggesting that a window for dislocation-free, tensile island growth is common to a broad range of (111) surfaces. These prior works used indirect bandgap materials that did not exhibit light emission, in contrast to the luminescent GaAs/InAlAs(111)B Q-dashes reported here.

Room temperature PL measurements of the GaAs Q-dashes are shown in Fig. 4. PL emission from the InAlAs matrix varies from 1.44 to 1.47 eV among the samples due to small variations in growth temperature,¹⁷ as discussed above. A strong GaAs Q-dash peak appears at 1.31 eV in the 2 ML GaAs sample and gradually red-shifts to 1.18 eV as the GaAs deposition increases to 4 ML, due to the quantum size effect. At 4 ML, the intensity of the GaAs PL decreases relative to the InAlAs peak due to the onset of dislocations in the GaAs layer. No GaAs PL was detected for the 1 ML sample due to insufficient confinement of carriers in the very thin GaAs. All of the GaAs Q-dash emissions are far below the GaAs bulk bandgap (1.42 eV) due to high tensile strain from the 3.8% lattice mismatch. In comparison, unstrained GaAs quantum wires grown within AlGaAs barriers always have emission energies higher than the bandgap due to quantum confinement (e.g., 1.48 eV in Ref. 25). In addition to direct bandgap energy reduction, high tensile strain is also expected to significantly reduce the bandgap of the indirect valleys.^{13,26} Strong PL observed at 10–300 K from the GaAs

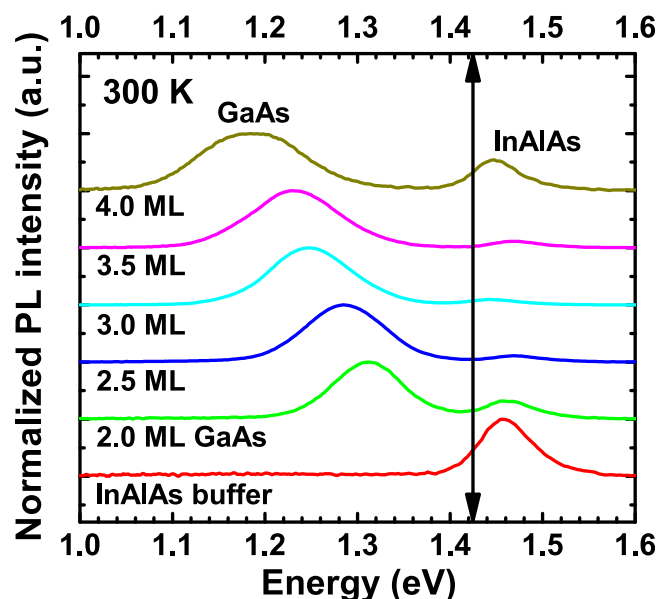


FIG. 4. Room-temperature PL spectra of tensile GaAs Q-dashes embedded within 600 nm thick InAlAs(111)B. The energy of the Q-dash emission red-shifts with the increase in GaAs thickness. Due to the tensile strain, the emission from the GaAs Q-dashes lies below the bulk GaAs bandgap (black arrow at 1.42 eV) in all samples.

Q-dashes suggests that the tensile GaAs remains in the direct bandgap regime (see supplementary material²¹). However, further work will be necessary to confirm the nature of the bandgap.

To corroborate the experimental Q-dash transition energies, we have estimated the ground state emission energy for the 3 ML Q-dashes, assuming a direct bandgap. A simple “particle in a finite box” model was used to calculate the electron and hole energies, simplifying the Q-dash geometry to that of a rectangular prism with dimensions taken from the TEM images of Figs. 3(d)–3(e). The calculated confinement energies are shown in Fig. 1, which assumes that the Q-dashes are fully strained biaxially to the InAlAs on InP. We calculate a transition energy of 1.15 eV for the 3 ML Q-dashes, compared to the experimental PL value of 1.24 eV. An underestimate of the Q-dash transition energy is expected for two reasons. First, partial elastic strain relaxation occurs during the 3D growth of the Q-dashes, which increases their bandgap.¹⁵ Second, the simplified box-geometry underestimates the quantum confinement experienced by electrons and holes. Numerical modeling of the wavefunctions according to the strain profile and the exact shape of the dashes is needed to calculate the PL energy more accurately.¹⁵ The Q-dash PL, nonetheless, shows reasonable agreement with the transition energy expected due to the interplay between tensile strain and confinement. Control over PL energy using tensile strain complements the use of quantum confinement in the Q-dashes, while extending the photon energies accessible to GaAs.

Finally, we investigated the presence of optical polarization in the tensile GaAs/InAlAs(111)B Q-dashes at 10 K. For the 4 ML GaAs sample, the PL of the tensile Q-dashes is slightly polarized perpendicular to the long axis of the dashes in the $[2\bar{1}\bar{1}]$ direction, unlike conventional unstrained²⁷ or compressively strained²⁸ quantum wires which emit light polarized parallel to their long-axes. However, the InAlAs matrix also exhibits polarized luminescence,²⁷ which influences the polarization of the embedded Q-dashes in thinner GaAs layers, similar to the report by Sugisaki *et al.*²⁹ Details on the complex polarization behavior of the tensile GaAs/InAlAs Q-dashes will be reported elsewhere.³⁰

This work has demonstrated the self-assembled growth of Q-dashes under large tensile strain, using (111)B oriented substrates to inhibit dislocation formation. The high material quality and strong type-I confinement induced by the tensile strain results in bright room temperature PL from the GaAs Q-dashes. Due to the 3.8% tensile lattice mismatch accommodated by the nanostructures, the GaAs bandgap decreases, emitting light 110–240 meV below the unstrained bandgap. Combined with previous work on GaP/GaAs(111)A²³ and Si/Ge(111),²⁴ the present work confirms that (111) surfaces generally support the growth of defect-free zinc-blende and diamond-cubic nanostructures under large tensile strain. The large bandgap reductions achievable using tensile strain are anticipated to extend quantum dot and quantum dash devices into longer wavelength ranges difficult to achieve by other means.

Microscopy facilities used in this work were supported by the Yale Institute for Nanoscience and Quantum Engineering and National Science Foundation MRSEC DMR 1119826. C.D.Y. acknowledges support from the Department of Energy Office of Science Graduate Fellowship Program (DOE SCGF), made possible in part by the American Recovery and Reinvestment Act of 2009, administered by ORISE-ORAU under Contract No. DE-AC05-06OR23100.

- ¹P. J. A. Thijs, J. J. M. Binsma, L. F. Tiemeijer, and T. Vandongen, *Electron Lett.* **28**, 829 (1992).
- ²S. Seki, T. Yamanaka, W. Lui, Y. Yoshikuni, and K. Yokoyama, *IEEE J. Quantum Electron.* **30**, 500 (1994).
- ³E. P. Oreilly, G. Jones, A. Ghiti, and A. R. Adams, *Electron Lett.* **27**, 1417 (1991).
- ⁴R. E. Camacho-Aguilera, Y. Cai, N. Patel, J. T. Bessette, M. Romagnoli, L. C. Kimerling, and J. Michel, *Opt. Express* **20**, 11316 (2012).
- ⁵D. Bimberg and U. W. Pohl, *Mater. Today* **14**, 388 (2011).
- ⁶J. P. Reithmaier, G. Eisenstein, and A. Forchel, *Proc. IEEE* **95**, 1779 (2007).
- ⁷T. C. Lin, Y. H. Wu, L. C. Li, Y. T. Sung, S. D. Lin, L. Chang, Y. W. Suen, and C. P. Lee, *J. Appl. Phys.* **108**, 123503 (2010).
- ⁸D. Pachinger, H. Groiss, M. Teuchtmann, G. Hesser, and F. Schaffler, *Appl. Phys. Lett.* **98**, 223104 (2011).
- ⁹P. J. Simmonds and M. L. Lee, *J. Appl. Phys.* **112**, 054313 (2012).
- ¹⁰Strained III-V bandgaps were calculated using the procedure given in Ref. 13 with material parameters from Ref. 14.
- ¹¹G. Signorello, S. Karg, M. T. Bjoerk, B. Gotsmann, and H. Riel, *Nano Lett.* **13**, 917 (2013).
- ¹²P. J. Simmonds, C. D. Yerino, M. Sun, B. Liang, D. L. Huffaker, V. G. Doring, Y. Mazur, G. Salamo, and M. L. Lee, *ACS Nano* **7**, 5017 (2013).
- ¹³C. G. Van de Walle, *Phys. Rev. B* **39**, 1871 (1989).
- ¹⁴T. Vurgaftman, J. R. Meyer, and L. R. Ram-Mohan, *J. Appl. Phys.* **89**, 5815 (2001).
- ¹⁵M. Grundmann, O. Stier, and D. Bimberg, *Phys. Rev. B* **52**, 11969 (1995).
- ¹⁶W. Yeo, R. Dimitrov, W. J. Schaff, and L. F. Eastman, *Appl. Phys. Lett.* **77**, 4292 (2000).
- ¹⁷R. Houdre, F. Gueissaz, M. Gailhanou, J. D. Ganiere, A. Rudra, and M. Illegems, *J. Cryst. Growth* **111**, 456 (1991).
- ¹⁸K. Inoue, K. Kimura, K. Maehashi, S. Hasegawa, H. Nakashima, M. Iwane, O. Matsuda, and K. Murase, *J. Cryst. Growth* **127**, 1041 (1993).
- ¹⁹H. Dery, E. Benisty, A. Epstein, R. Alizon, V. Mikhelashvili, G. Eisenstein, R. Schwertberger, D. Gold, J. P. Reithmaier, and A. Forchel, *J. Appl. Phys.* **95**, 6103 (2004).
- ²⁰G. D. Lian, J. Yuan, L. M. Brown, G. H. Kim, and D. A. Ritchie, *Appl. Phys. Lett.* **73**, 49 (1998).
- ²¹See supplementary material at <http://dx.doi.org/10.1063/1.4893747> for TEM observation of dislocation formation and for temperature-dependent PL data.
- ²²L. Goldstein, F. Glas, J. Y. Marzin, M. N. Charasse, and G. Leroux, *Appl. Phys. Lett.* **47**, 1099 (1985).
- ²³P. J. Simmonds and M. L. Lee, *Appl. Phys. Lett.* **99**, 123111 (2011).
- ²⁴A. Raviswaran, C. P. Liu, J. Kim, D. G. Cahill, and J. M. Gibson, *Phys. Rev. B* **63**, 125314 (2001).
- ²⁵E. Kapon, S. Simhony, R. Bhat, and D. M. Hwang, *Appl. Phys. Lett.* **55**, 2715 (1989).
- ²⁶G. E. Chang and H. H. Cheng, *J. Phys. D: Appl. Phys.* **46**, 065103 (2013).
- ²⁷F. Vouilloz, D. Y. Oberli, M. A. Dupertuis, A. Gustafsson, F. Reinhardt, and E. Kapon, *Phys. Rev. B* **57**, 12378 (1998).
- ²⁸C. Constantin, E. Martinet, F. Lelarge, K. Leifer, A. Rudra, and E. Kapon, *J. Appl. Phys.* **88**, 141 (2000).
- ²⁹M. Sugisaki, H. W. Ren, S. V. Nair, K. Nishi, S. Sugou, T. Okuno, and Y. Masumoto, *Phys. Rev. B* **59**, R5300 (1999).
- ³⁰V. G. Doring, M. E. Ware, Y. I. Mazur, C. D. Yerino, P. J. Simmonds, B. Liang, D. L. Huffaker, G. Salamo, and M. L. Lee (unpublished).